Contents lists available at SCCE

Journal of Soft Computing in Civil Engineering

Journal homepage: www.jsoftcivil.com

Predicting Post-Fire Behavior of Green Geopolymer Mortar Containing Recycled Concrete Aggregate via GEP Approach

Sh. Fakhrian[1*], H. Behbahani[2], Sh. Mashhadi[3]

1. M.Sc., Department of Civil Engineering, Faculty of Engineering and Technology, Maziar University, Royan, Iran
2. Professor, Department of Road and Transportation, School of Civil Engineering, Iran University of Science and Technology, Tehran, Iran
3. M.Sc., Department of Petroleum Engineering, Faculty of Chemical Engineering, Tarbiat Modares University, Tehran, Iran

Corresponding author: *fakhrian.architect@yahoo.com*

https://doi.org/10.22115/SCCE.2020.220919.1182

ARTICLE INFO

Article history:
Received: 01 March 2020
Revised: 19 April 2020
Accepted: 21 April 2020

Keywords:
Geopolymer mortar;
Recycled concrete aggregate;
Elevated temperatures;
Gene expression programming.

ABSTRACT

In the present study, 20 models were developed using gene expression programming (GEP) to predict the compressive strength and mass loss of geopolymer mortar (GPM) containing recycled concrete aggregate (RCA) exposed to elevated temperatures. To do so, the results of 160 specimens manufactured out of 32 different mixture designs in an experimental effort were used. In developing the models, 80% of the total datasets were employed in the training phase, with the remaining 20% used in the validation phase. Three input variables were taken into account, namely the applied temperature (T), recycled concrete aggregate (RCA) replacement level, and superplasticizer (SP) addition percentage. The training and validation phases with the coefficient of determination of 0.95 to 0.99 demonstrated that there was proper consistency between results predicted by the proposed models and the experimental results. Moreover, the results of statistical analyses gave another reason for the ability of GEP to predict both the compressive strength and mass loss of GPM containing recycled concrete aggregate under elevated temperatures.

1. Introduction

Increasing costs and depleting natural resources have forced humanity to turn towards recycling and reusing waste materials. Although this issue has become relevant to the construction industry

How to cite this article: Fakhrian Sh, Behbahani H, Mashhadi Sh. Predicting post-fire behavior of green geopolymer mortar containing recycled concrete aggregate via GEP approach. J Soft Comput Civ Eng 2020;4(2):22–45. https://doi.org/10.22115/SCCE.2020.220919.1182.

in recent years, the use of recycled waste materials in this industry has not yet become commonplace around the world. In this regard, one strategy is to use construction and demolition (C&D) waste materials as alternative aggregates in new concrete [1,2]. With regard to a lower quality of recycled aggregate concrete (RAC) compared with conventional concrete, many experimental efforts have been conducted by researchers to find solutions for improving the RAC quality. It has been demonstrated that using recycled concrete aggregate (RCA) in concrete lowers the elastic modulus, compressive strength, and freeze-thaw resistance while increasing the creep, drying shrinkage, water absorption, and carbonation speed in comparison with using natural aggregate. However, these properties can be enhanced through designing a proper mix and adding mineral admixtures [3].

Portland cement (PC) is a commonly used material as the main binder in construction activities. Estimates say that around 12–15% of the entire industrial energy input is consumed in the cement production [4]. Along with technological progress in PC production, the associated energy consumption, together with adverse emissions, have declined. Nevertheless, even the most efficient cement production facilities still consume up to 4 GJ energy and release around one ton carbon dioxide (CO_2) per each ton of cement produced [5]. As a result, cement production industry is responsible for a huge volume of greenhouse gas (GHG) emissions into the atmosphere, which in turn exacerbates the climate change effects. Considering the fact that protecting the environment is becoming more and more important, discovering a viable alternative to PC seems to be of particular significance. In this regard, to replace ordinary Portland cement (OPC), geopolymer materials have emerged as likely options [6–8].

Employing geopolymer materials has advantages regarding environmental protection since doing so curbs greenhouse gases (GHGs) released due to producing cement [9]. Multiple industrial by-products can be used as geopolymers, namely ground granulated blast furnace slag and fly ash [10–12]. To make slag-based geopolymer concrete (GPC), alkaline solutions including sodium silicate (Na_2SiO_3) and sodium hydroxide (NaOH) can be utilized to activate the slag [6]. A number of factors affect the mechanical properties of slag-based GPC, which include the type of alkali activator solution and its dosage, raw materials, curing conditions, and solution-to-binder ratio. [13–16]. Due to its quick strength attainment, the initial strength of slag-based GPC is a rather high, such that the one-day strength can reach up to 60 MPa [17]. A majority of studies in the literature have found the elastic modulus of slag-based GPC to be near that calculated for OPC concrete by different codes in the range of 10–40 GPa [17–19]. Furthermore, during the hydration of geopolymer materials, the main product is calcium aluminosilicate hydrate (C-A-S-H). As reported by Walkley et al. [20], the principal product of the reaction of any geopolymer material is a cross-linked sodium- and aluminum-substituted calcium silicate hydrate (C-(N)-A-S-H)-type gel. In addition, As reported by Myers et al. [21], the principal substance formed during the activation of blast furnace slag is a calcium aluminosilicate hydrate (C-A-S-H) gel.

In general, when conventional concrete is subjected to high temperatures, strength loss occurs due to the hydrogen decomposition in $Ca(OH)_2$, C-S-H phase, and other hydrated compounds [22]. In the study of Peng et al. [23], the decomposition of C–S–H began at 560 ℃, and it converted to C_2S and C_3S at 800 ℃. It was also found that the content of $Ca(OH)_2$ in

conventional concrete declined when the applied temperature went above 450 ℃. Many researchers have focused on the resistance of slag-based GPC to high temperatures. Given that slag-based GPC lacks $Ca(OH)_2$, it is expected to demonstrate better behavior relative to OPC concrete during fire [24]. The superior resistance of slag-based GPC to high temperatures is associated with the content of $Ca(OH)_2$ in slag-based geopolymer paste. Jumppanen et al. [25] noted that after hydration, the content of $Ca(OH)_2$ in slag-based geopolymer pastes is low, thus $Ca(OH)_2$ dehydroxylation does not control their performance in fire. Hence, the spalling resistance of slag-based GPC in fire is greater than conventional concrete. Mao-Chieh Chi et al. [26] attributed the higher strength of geopolymers relative to cement mortars to the different structure and composition of the formed C-S-H. The properties of sodium silicate-activated geopolymer materials after exposure to temperatures of up to 1200 ℃ were addressed by Zuda et al. [27]. The findings suggested the significant capacity of these materials for use in practical applications. Following heating at elevated temperatures, it was observed that in the binder, the calcium silicate hydrate (C-S-H) matrix was slowly replaced with a new akermanite-based structure.

Moreover, after heating up to 1200 ℃, the porosity of the materials increased significantly. In another work, the researchers observed both thermal conductivity and thermal diffusivity of slag-based geopolymer materials to decline after the exposure increased above 400 ℃; hence, the effectiveness of these materials for high-temperature applications is resulted [28]. Guerrieri et al. [29] addressed the residual compressive strength of OPC concrete, mixed OPC/slag (50/50) concrete, and slag-based GPC activated by sodium silicate and hydrated lime after experiencing high temperatures of up to 1200 ℃. Based on the findings, although the slag-based GPC lacked $Ca(OH)_2$, it exhibited proper behavior in the temperature range of 400-800 ℃, which was consistent with the results of the OPC and the mix slag/cement concretes. The authors attributed the reduction in the strength of slag-based GPC activated by powdered sodium silicate and hydrated lime at high temperatures to greater thermal incompatibility of aggregate-slag-based geopolymer paste, which was notably greater than that in the concretes containing other binders. In another work, Guerrieri et al. [30] addressed the strength of slag-based geopolymer paste activated by sodium silicate after exposure to heat. Based on the findings, the slag-based geopolymer paste experienced a fast strength reduction of around 60% when exposed to 100 and 200 ℃, and a further strength reduction of around 30% at 800 ℃. After exposure to 1200 ℃, total strength loss occurred.

As the volume of waste concrete obtained after the repair and renovation of deteriorating infrastructures increases, finding sites to dispose of waste materials has become a challenge [31]. Moreover, a huge volume of natural aggregate is required for concrete production, which is, in turn, diminishing natural aggregate (NA) sources at a rapid rate, leading to environmental issues [32]. Therefore, the use of RCA in concrete is becoming more widespread as a viable solution for environmental problems associated with waste materials. This strategy can alleviate stress on natural aggregate quarries and waste landfills and protect the environment in return. In general, concrete made with RCA has shown a lower compressive strength relative to concrete made with NA [33]; however, the results of experiments conducted by Kathirvel et al. [34] demonstrated that by using 50% RCA in the mix, the compressive strength and water absorption of slag-based

GPC increased. Kathirvel et al. [35] addressed the variation of engineering and durability properties of slag-based GPC containing RCA cured under ambient conditions. Here, slag-based GPC mixes with different fractions of RCA replacing NA, namely 0, 25, 50, 75, and 100%, were examined. The concretes where 50 and 100% of NA were replaced with RCA demonstrated the greatest strength and the better behavior relative to the OPC concrete, respectively. Shi Cong Kou et al. [36] observed that in comparison with the concrete containing NA, the concrete containing RCA experienced fewer mechanical and durability properties reductions after exposure to heat. Several studies have already addressed the performance of slag-based GPC containing RCA under high temperatures. However, the performance of slag-based geopolymer mortar (GPM) made with RCA in fire and the thermal compatibility between the aggregate and the slag-based geopolymer paste have not been investigated.

Given the cost- and time-consuming nature of fabricating concrete artifacts in the laboratory to determine the mechanical properties, especially durability, in this work, the authors employed soft computing methods for predicting post-fire properties of GPM fabricated with RCA. Furthermore, to predict various concrete properties, a number of these techniques including fuzzy logic [37,38], artificial neural networks [39–44], nature-inspired algorithms [45,46] and genetic algorithms [47–51] have already been utilized in the literature. As a somewhat new modeling technique, gene expression programming (GEP) [52] has been shown to be better able to obtain mathematical relationships for experimental results than conventional regression techniques and neural networks [53,54]. With respect to the aforementioned discussion, this study attempted to contribute to filling the above research gap by developing accurate models for predicting the post-fire GPM properties. In this regard, the materials used in making green mortar and the method employed to develop the prediction models make this study a novel one regarding the prediction models for the mortar post-fire properties. GEP was used for the first time in the current work to examine the compressive strength and mass loss of slag-based GPM containing RCA after exposure to heat.

2. Utilized Data

The data of an experimental program were utilized for training and validating GEP models. The goal of this work was to explore the effect of RCA inclusion on the compressive strength and fire resistance of slag-based GPM exposed to high temperatures to be able to improve the aggregate-slag-based geopolymer paste compatibility. In the experimental program, the residual compressive strength and other properties of the slag-based GPM containing 11 different replacement ratios of RCA, namely 0, 10, 20, 30, 40, 50, 60, 70, 80, 90, and 100%, were explored after exposure to the ambient temperature of 23 and high temperatures of 200, 400, 600, and 800 °C. To that end, the compressive strength and the mass loss were measured after thermal loading. According to the results, the use of 30% RCA in the slag-based GPM enhanced the behavior at ambient and high temperatures. In addition, as observed in the petrographic images, the cohesion between RCA and slag-based geopolymer paste was stronger at high temperatures. Altogether, using these two material types, namely slag, and RCA, in combination, shows a high ability to promote producing clean, sustainable, and eco-friendly green mortar. The Supplementary File can be referred for more details regarding the experimental results. To better develop the models, the details of the experimental program are given below.

2.1. Materials

To manufacture the specimens, ground granulated blast-furnace slag (GGBFS) provided from Sepahan Cement Company, Isfahan, Iran, was used. GGBFS is a by-product of the steel production industry. For the slag, Table 1 shows the physical properties and chemical composition obtained from X-ray fluorescence test.

Table 1
Chemical and physical properties of slag.

Chemical Properties (%)			Physical Properties
CaO	SiO_2	MgO	Specific surface, Blaine (m^2/gr)
43.13	32.21	7.32	360
Al_2O_3	SO_3	TiO_2	Specific gravity
6.8	3.54	2.13	2.7
MnO	K_2O	Na_2O	Particle diameter (μm)
1.98	1.81	1	1-15

To activate GGBFS, a solution consisting of NaOH and Na_2SiO_3 mixed together was used as an activator. NaOH, 98%, extra pure in the form of flakes, was utilized. Moreover, the constituents of the Na_2SiO_3 solution by volume were 29.8% SiO_2, 10.2% Na_2O, and 60% H_2O; thus, the silica modulus was determined as 2.9. In compliance with ASTM C33 [55], Fig. 1 gives the upper and lower bounds for the size of NA and RCA in mixes.

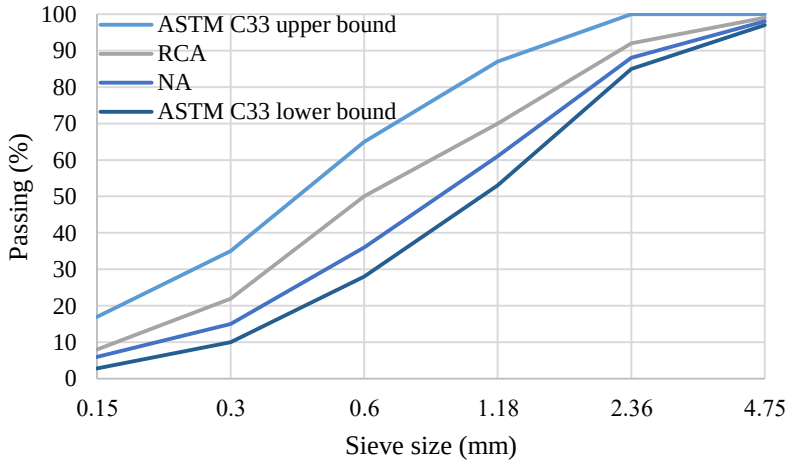

Fig. 1. The sieve analysis of NA and RCA and the upper and lower bounds according to ASTM C33.

River sand was employed as the NA, and fine aggregate was RCA obtained from concrete waste. Table 2 gives the characteristics of RCA and NA.

Table 2
Characteristics of NA and RCA.

Aggregate	Bulk density (Kg/m^3)	Specific gravity	Water absorption (%)	Fineness modulus
NA	1680	2.66	1	2.94
RCA	1376	2.34	2.5	2.6

Note that water absorption of fine aggregate was considered in the calculations, and the aggregate particles were in the saturated-surface-dry (SSD) condition. Moreover, a

polycarboxylate-based liquid superplasticizer (SP) with 40% solid content was poured to obtain a suitable workability, determined by the flow cone test, as suggested by ASTM C230 [56].

2.2. Preparing mortar

Ten different RCA replacement ratios were considered to prepare the slag-based GPM mixes. The mixes were made by replacing 0, 10, 20, 30, 40, 50, 60, 70, 80, 90, and 100% of the NA volume with RCA, which were labeled as RA^{0}, RA^{10}, RA^{20}, RA^{30}, RA^{40}, RA^{50}, RA^{60}, RA^{70}, RA^{80}, RA^{90}, and RA^{100}, respectively. In addition, the slag-sand and water-solids ratios was 0.4 and 0.42, respectively. Table 3 gives the fractions of different constituents in the mortar mixes.

Table 3
The mixture proportions used for the slag-based GMP.

Mixture	Water/Solids	Na_2SiO_3 solution (g)	NaOH solution (g)	Slag (g)	RCA (g)	NA (g)	SP (%)
RA^{0}	0.42	191.25	63.75	510	0	1275	0
RA^{0}_{+1}					0	1275	0.01
RA^{10}_{-1}					127.5	1147.5	0.01
RA^{10}					127.5	1147.5	0.02
RA^{10}_{+1}					127.5	1147.5	0.03
RA^{20}_{-1}					255	1020	0.03
RA^{20}					255	1020	0.04
RA^{20}_{+1}					255	1020	0.05
RA^{30}_{-1}					382.5	892.5	0.05
RA^{30}					382.5	892.5	0.06
RA^{30}_{+1}					382.5	892.5	0.07
RA^{40}_{-1}					510	765	0.07
RA^{40}					510	765	0.08
RA^{40}_{+1}					510	765	0.09
RA^{50}_{-1}					637.5	637.5	0.09
RA^{50}					637.5	637.5	0.10
RA^{50}_{+1}					637.5	637.5	0.11
RA^{60}_{-1}					765	510	0.11
RA^{60}					765	510	0.12
RA^{60}_{+1}					765	510	0.13
RA^{70}_{-1}					892.5	382.5	0.13
RA^{70}					892.5	382.5	0.14
RA^{70}_{+1}					892.5	382.5	0.15
RA^{80}_{-1}					1020	255	0.15
RA^{80}					1020	255	0.16
RA^{80}_{+1}					1020	255	0.17
RA^{90}_{-1}					1147.5	127.5	0.17
RA^{90}					1147.5	127.5	0.18
RA^{90}_{+1}					1147.5	127.5	0.19
RA^{100}_{-1}					1275	0	0.19
RA^{100}					1275	0	0.20
RA^{100}_{+1}					1275	0	0.21

The preparation procedure of the alkaline solution was as follows: NaOH was diluted in water and put at ambient temperature for 24 hours; this was done to decrease the rapid setting of the solution as a result of heat. Note that the concentration was constant and equal to 12 M. Afterward, the NaOH solution was mixed with Na_2SiO_3, with the Na_2SiO_3/NaOH ratio of 3. Table 4 gives the mix design parameters that were constant for all slag-based GPM mixes.

Table 4
Constant parameters for slag-based GPM mixes.

Parameter	Value
Na_2SiO_3/NaOH solution ratio	3
Sand-slag ratio	2.5
Alkali solution-slag ratio	0.5
NaOH solution concentration (M)	12
Water-solids ratio	0.42

The ASTM C305 [57] recommendations was followed in the preparation of the slag-based GPM. The next step was casting the fresh mortar in molds with oiled inner surfaces and curing them for 24 hours. Finally, all the specimens were demolded and cured for 28 days in wet conditions.

2.3. Test procedure

The compression tests were conducted on the 50 × 50 × 50 mm cubic mortars specimens prior to and following thermal loading in compliance with ASTM C109 [58]. The specimens were kept in the laboratory environment after the end of the 28-day curing. For thermal loading, the specimens were put in an electric furnace and heated at a thermal loading rate of 5 °C/min and 2 hours soaking time until reaching the target temperature. To achieve a steady-state thermal distribution, the specimens were maintained in the furnace for two hours. Then, the furnace was switched off, and the specimens were left in it for 24 h to slowly cool down. Finally, the residual compressive strength and mass loss were measured. Note that to reduce error, for each individual mix, three similar specimens were tested, for which the mean of the measured values was considered and reported in the paper.

3. GEP models and parameters

3.1. Gene expression programming

Koza [59] proposed genetic programming (GP) in 1992 as a branch of genetic algorithms (GAs). GP and GAs differ from each other mainly in terms of how the solution is represented, in that the solution to GP is a computer program while the solution of GA is a string of numbers Gene expression programming (GEP) is a linear variant of GP. Linear variants of GP clearly differentiate between the genotype and phenotype of an individual. In GP's linear variants, linear strings are used to represent the individuals [60]. GEP has five main components which include function set, terminal set, fitness function, control parameters, and stop criterion. For representing a solution to a problem, GEP employs a fixed length of character strings, contrary to the parse-tree representation in conventional GP. Computer models in tree-like structures [expression trees (ETs)] are used to further show the solutions. GEP is advantageous in many respects one of which is the highly simplified generation of genetic diversity, due to the function of genetic operators at chromosome level. Also, GEP has a specific multi-genic feature, allowing programs of greater complexity consisting of multiple sub-programs to evolve. Every GEP gene has a list of fixed-length symbols which can be any element from the function and terminal sets. Fundamental mathematical operators (+, −, *, /) or any other function defined by user can be in the function set. However, numerical and logical constants or variables can exist in the terminal set. The function set and terminal set must have the closure property; each function must be able

to take any value of data type that can be returned by a function or assumed by a terminal. What follows is a typical GEP gene having specified terminal and function sets, $/.log.+.+.a.5.b.c$, where a, b and c are variables, and 5 is a constant. To be able to read easily, the periods are used to separate the elements. Karva notation or K-expression is a name given to the preceding expression. Conversion is the term given to the information decoding process from K-expression to expression trees is called. This process is conducted according to sets of rules, and it begins from the first location in the K-expression, corresponding to the root of the ET, and then reads through the string one by one. For instance, Fig. 2 gives a typical representation of the preceding sample gene, where a–c are variables + and / are the plus and division signs, respectively).

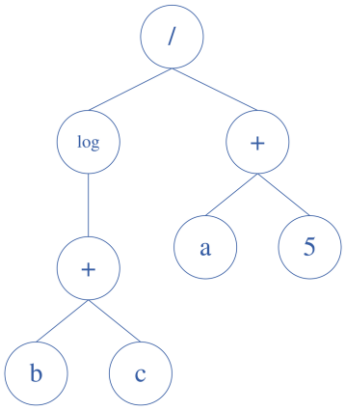

Fig. 2. Typical illustration of an expression tree.

Moreover, the mathematical representation for the preceding GEP gene is as follows, $log(b + c) / (a + 5)$, where a, b, and c are variables. The inverse conversion of an ET into a K-expression is possible. To do this, in each ET layer from root layer down to the deepest layer, the nodes are recorded from left to right form the string. GEP genes are fixed in length, which is predetermined for a given problem, as mentioned above. Therefore, in GEP, the gene lengths are invariant, and the sizes of the corresponding ETs are those that vary. It implies the existence of a number of redundant elements not beneficial for mapping the genome. Therefore, the valid length of a K-expression can be the same as or smaller than that of the GEP gene. GEP uses a head–tail approach to ensure that a genome selected randomly is valid. Every gene in GEP consists of a head and a tail. The head includes a number of mathematical operators, variables, and constants (+, −, *, /, sin, cos, 1, a, b and c) utilized for encoding a mathematical formula, while the tail only involves constants and variables (1, a, b and c) known as terminal symbols [60].

Fig. 3 gives a schematic illustration of the basic steps of GEP. In GEP, the roulette wheel sampling with elitism is used to select and copy the individuals into the next generation according to the fitness [61]. Doing so ensures the survival and cloning of the best individual to the next generation. By performing one or more genetic operations on chosen chromosomes, variation is introduced in the population. These operations involve crossover, mutation, and rotation. Via the rotation, two subparts of the element sequence in a genome are rotated with respect to a point selected randomly. This operation is also capable of considerably reshaping the ETs [62].

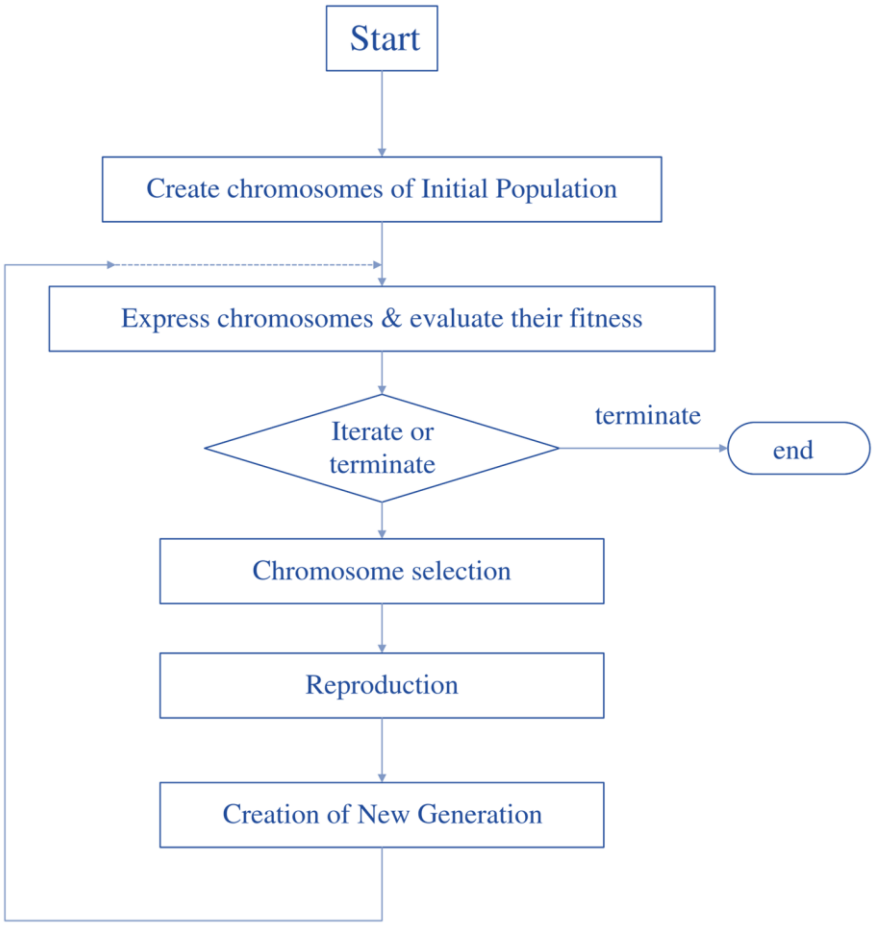

Fig. 3. The flowchart of a GEP algorithm.

The GEP model development procedure can include the following steps [63]:

a. Choosing the fitness function,
b. Selecting the functions set and the terminals set to obtain chromosomes,
c. Selecting the architecture of chromosomes,
d. Selecting the linking function, and
e. Selecting the genetic operators.

3.2. Proposed models and statistical parameters

This study was the first attempt to utilize the GEP modeling for predicting the compressive strength and mass loss of the slag-based GPM containing RCA exposed to elevated temperatures. The tool used to model data was the GeneXproTools program [64]. Here, the loss of mass and strength were estimated via taking various parameters into account. In the end, a comparison was made between the modeling and empirical results.

An experimental procedure was carried out on specimens with different variables, so that the two above properties could be predicted. The input variables were the exposure temperature (T), recycled concrete aggregate (RCA) replacement level, and superplasticizer (SP) content, and the output variables were the compares strength and loss of mass. Table 5 gives the lower and upper boundaries for the input and output variables. For the models, eighty percent of the specimens

from the total dataset were selected randomly as the training set, with the other twenty percent employed as the testing set.

Table 5
Boundaries of input and output variables employed in GEP modeling.

Input variables	Lower bound	Upper bound
Applied heat (°C)	23	800
RCA replacement (%)	0	100
Superplasticizer (%)	0	0.2
Output variables		
Compressive strength (MPa)	4.8	66.3
Mass loss (%)	0	14.08

Here, twenty GEP models, namely *GEP1* to *GEP20*, were utilized. Among the GEP models, those with higher coefficients of determination were selected. Then, the selected models were evaluated against each other to assess the impact of elevated temperatures and RCA content on the strength and mass loss of slag-based GPM. To obtain the minimum error, the stiffness function having the best fitness was chosen. For statistical evaluation of errors occurring inevitably, five stiffness functions were used in the training and testing phases. These functions were the absolute fraction of variance (R^2), root mean square error (RMSE), mean absolute error (MAE), relative absolute error (RAE), and root relative squared error (RRSE), expressed as Eqs. (2)-(6), respectively.

$$R^2 = \frac{\left(n\sum t_i o_i - \sum t_i \sum o_i\right)^2}{\left(n\sum t_i^{\,2} - \left(\sum t_i\right)^2\right)\left(n\sum o_i^{\,2} - \left(\sum o_i\right)^2\right)} \tag{2}$$

$$MAE = \frac{1}{n}\sum_{i=1}^{n}\left|t_i - o_i\right| \tag{3}$$

$$RMSE = \sqrt{\frac{1}{n}\sum_{i=1}^{n}\left(t_i - o_i\right)^2} \tag{4}$$

$$RAE = \frac{\sum_i \left|t_i - o_i\right|}{\sum_i \left|t_i - (1/n)\sum_i t_i\right|} \tag{5}$$

$$RRSE = \sqrt{\frac{\sum_i \left(t_i - o_i\right)^2}{\sum_i \left(t_i - (1/n)\sum_i t_i\right)^2}} \tag{6}$$

In the above equations, o, t, and n are the output value, target value, and number of all the collected data, respectively. The aim of considering all these error values is choosing the best model. The presentation of models were conducted based on the parameters and functions with and without considering the weight of the functions given in Table 6. It should be noted in all

approaches the values of mutation, inversion, and transposition have been considered as 0.044, 0.1, and 0.1, respectively.

Table 6
Utilized parameters for each GEP approach.

Models set	Chromosomes	Head size	Number of genes	Linking function	Fitness function	Constant per gene	Number of functions
GEP1	30	10	3	Addition	Absolute error with SR	2	6[a,1]
GEP2	26	12	3	Multiplication	Absolute error with SR	2	6[a,1]
GEP3	40	14	4	Addition	Absolute error with SR	2	6[a,1]
GEP4	35	12	3	Multiplication	Absolute error with SR	2	7[b,1]
GEP5	35	8	3	Addition	Absolute error with SR	2	8[c,2]
GEP6	30	12	3	Addition	Absolute error with SR	2	4[d,1]
GEP7	30	8	2	Addition	Absolute error with SR	2	6[a,1]
GEP8	30	10	3	Addition	Absolute error with SR	2	6[a,1]
GEP9	40	12	4	Addition	Absolute error with SR	1	10[e,4]
GEP10	30	9	3	Addition	Absolute error with SR	2	7[b,1]
GEP11	60	8	3	Addition	Absolute error with SR	2	7[f,1]
GEP12	30	10	3	Addition	Absolute error with SR	2	13[g,1]
GEP13	30	8	3	Addition	RRSE	2	8[c,1]
GEP14	30	8	3	Addition	RRSE	1	4[h,1]
GEP15	30	8	3	Addition	RRSE	2	7[b,1]
GEP16	30	12	3	Multiplication	RRSE	2	9[i,2]
GEP17	30	10	3	Addition	RRSE	2	6[j,3]
GEP18	40	12	4	Addition	RRSE	1	8[k,4]
GEP19	30	12	3	Addition	RRSE	2	13[g,1]
GEP20	30	12	3	Addition	RRSE	2	12[l,4]

[1] The "+, −, ∗" functions had a weight 4 times weight of other functions
[2] The "+, −, ∗" functions had a weight 7 times weight of other functions
[3] The "∗" function had a weight 4 times weight of other functions
[4] The "+, −, ∗" functions had a weight 3 times weight of other functions
[a] The +, −, ∗, /, *sqrt*, x^3 functions were employed
[b] The +, −, ∗, /, *sqrt*, x^3, x^2 functions were employed
[c] The +, −, ∗, /, *sqrt*, x^3, x^2, *3Rt* functions were employed
[d] The +, −, ∗, / functions were employed
[e] The +, −, ∗, /, *sqrt*, *exp*, *sin*, *cos*, *atan*, *ln* functions were employed
[f] The +, −, ∗, *sqrt*, x^3, x^2, *3Rt* functions were employed
[g] The +, −, ∗, /, *sqrt*, x^5, x^4, x^3, x^2, *3Rt*, *4Rt*, *5Rt*, *ln* functions were employed
[h] The +, −, ∗, /, *sqrt* functions were employed
[i] The +, −, ∗, /, *sqrt*, x^3, *exp*, *sin*, *cos* functions were employed
[j] The +, ∗, *sqrt*, x^3, x^2, *pow* functions were employed
[k] The +, −, ∗, /, *exp*, *sin*, *cos*, *atan* functions were employed
[l] The +, −, ∗, /, *sqrt*, x^4, x^3, x^2, *3Rt*, *4Rt*, *exp*, *ln* functions were employed

The GEP models were used to develop formulas in the form of Eq. (7) to determine the compressive strength and mass loss,

$$y = f\left(T, SP, RCA\right) \tag{7}$$

4. Results and discussion

Based on the above discussion, the formulas developed using the GEP models are expressed mathematically in Tables 7 and 8 and represented as ETs in Figs. 4 and 5. In the formulas given in the tables, d_0, d_1 and d_2 refer to T, SP and RCA, respectively. For compressive strength, Fig. 4 shows the expression trees of the best models, namely *GEP13*, *GEP16*, *GEP18* and *GEP19*. Also, for mass loss, Fig. 5 shows the ETs of the best models, namely to *GEP16*, *GEP18*, *GEP19* and *GEP20*.

Table 7
Mathematical formulas for compressive strength developed from GEP models.

Models set	Developed formulas for compressive strength
GEP13	$y = \sqrt[3]{{c_3}^3 \times d_0} \times \sqrt[3]{c_6 + d_1} + c_3 + \frac{c_3 + c_0 + d_0 + c_3}{c_6 + d_2/d_0} + c_3 \times \left(\frac{c_3 - d_1}{d_2 + c_0} + 2d_1 + c_6\right)$
GEP16	$y = \cos\left(\mathrm{e}^{(d_1 + d_2)} - d_0\right) + \cos\left(d_0\right) + \left(c_0 - c_1\right) \times \frac{c_1}{c_0} \times \cos\left({d_0}^2\right) \times \cos^3\left({d_0}^3 + 2d_1\right) + c_0 \times c_0 - \cos\left({d_0}^2\right) - \sin\left(\sin\left(\sin\left(d_1\right) - \left(d_0 - d_1\right)\right)\right)$
GEP18	$y = \sin\left(\left(\tan^{-1}\left(d_1\right) + \left(d_0 \times c_0\right)\right) + \left(\cos\left(d_2 - c_0\right)\right)\right) + \cos\left(2c_0 \times \left(d_0 + c_0\right)\right) + \sin\left(e^{(d_1 - d_0)} + \cos\left(c_0\right) + {d_0}^2\right) - \cos\left(\left(c_0 + d_2\right) - \left(d_0 \times c_0\right)\right) + e^{\left(\cos\left(d_1 + \left(e^{c_0} + c_0\right)\right) - \left(d1 + \left(2c_0 + \sin\left(d_0\right)\right)\right)\right)} + \sin\left(\left(\tan^{-1}\left(d_1\right) + \left(d_0 \times c_0\right)\right) + \cos\left(c_0 - d_0\right)\right) + \cos\left(\left(2c_0\right) \times \left(d_0 + c_0\right)\right)$
GEP19	$y = \left(\sqrt[3]{c_0} + \sqrt[3]{\sqrt[5]{\left(d_0 - d_1\right) - c_1} - c_1}\right)^3 + \left({c_0}^3 - \left(d_0 \times c_1\right) + 2d_1 + d_2\right)^{\frac{6}{3}} + \sqrt[6]{\left(\left(\left(d_2 - c_1\right) - \left(c_1 \times c_0\right)\right) \times \left(\left(c_0 - d_1\right) + \left({c_1}^2\right)\right) \times {c_0}^2\right)}$

C_0 = -6.64113284707175; C_3 = -5.82811975463118; C_6 = -6.25782036805322 for *GEP13*
C_0 = -0.746177556688131; C_1 = -5.28855250709555 for *GEP16*
C_0 = -1.31260109256264 for *GEP18*
C_0 = 8.82625812555315; C_1 = 1.45481734672079 for *GEP19*

Table 8
Mathematical formulas for mass loss developed from GEP models.

Models set	Developed formulas for mass loss
GEP16	$y=\cos\left(\cos\left(\sin^3\left(c_0+d_0\right)+\sin\left(c_1/d_0\right)+d_1\right)^3\right)\times \sqrt{d_0}-\cos\left(\left(\left(d_0-d_2\right)-\left(c_1+c_0\right)\right)-\left(d_2\times {d_1}^2\right)\right)-c_0\times \cos\left(\cos^3\left(\cos\left(\left(d_2\times {c_1}^3\right)+\left(c_0+d_2\right)\right)\right)\right)$
GEP18	$y=c_0\times\cos\left(d_2\right)+d_2/\left(c_0+c_0\times d_2\times {d_1}^2\right)+ \tan^{-1}\left(\left(\sin\left({d_0}^2\right)\times\left(d_1\times c_0-c_0\right)\right)-\tan^{-1}\left(d_2\times d_1-\tan^{-1}d_2\right)\right)+ c_0\times\cos\left(\left(d_0-d_1+\cos\left(c_0\right)\right)-\tan^{-1}\left(d_2+c_0\right)\right)-d_1+ \cos\left(c_0\times d_2\times\left(d_0-\left(2d_0-c_0\right)\right)\right)\times c_0$
GEP19	$y=\sqrt[3]{\sqrt[5]{d_2}-\left(d_2-c_1\right)^{\frac{5}{3}}/\left(\left(\frac{d_2}{d_0}\right)^3-\left(c_1-d_0\right)\right)}+ \sqrt[9]{d_0/\left(Ln\left(d_0-d_1\right)+\left(c_1-d_1\right)\right)+2c_1}+ \left(\sqrt{d_1}-2d_1\right)^{\frac{1}{8}}+\left(\sqrt{d_2+d_0}+d_0\right)^{\frac{1}{3}}$
GEP20	$y=e^{e^{\cos\left(c_1{}^3/\left(d_0-\left(e^{\cos(d_0)}-\sin(d_0)\right)\right)\right)}}+ e^{\sin\left(d_0+\left(d_0\times c_1-d_2\right)^3\times\left(c_0+d_0\right)^{\frac{3}{2}}\right)}+ \left(\left(\sin\left(\cos\left(d_0\right)\right)-\left(d_1\right)^{\frac{3}{2}}\right)-\left(e^{\sin(d_1)}-e^{\cos(d_0)}\right)\right)^3$

C_0 = 5.55833613086337; C_1 = -3.75041962950529 for *GEP16*
C_0 = 7.29911191137425; C_1 = 1.75695059053316 for *GEP18*
C_1 = -6.47633289590136 for *GEP19*
C_0 = -7.22037415692618; C_1 = -6.96462904751732 for *GEP20*

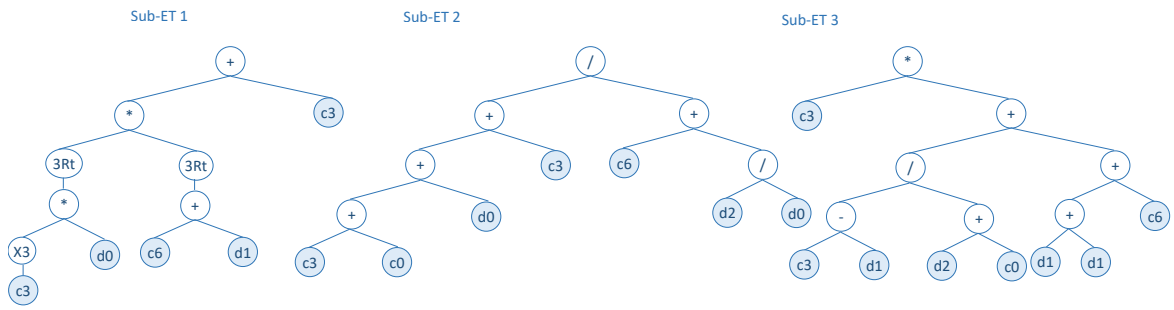

(a)

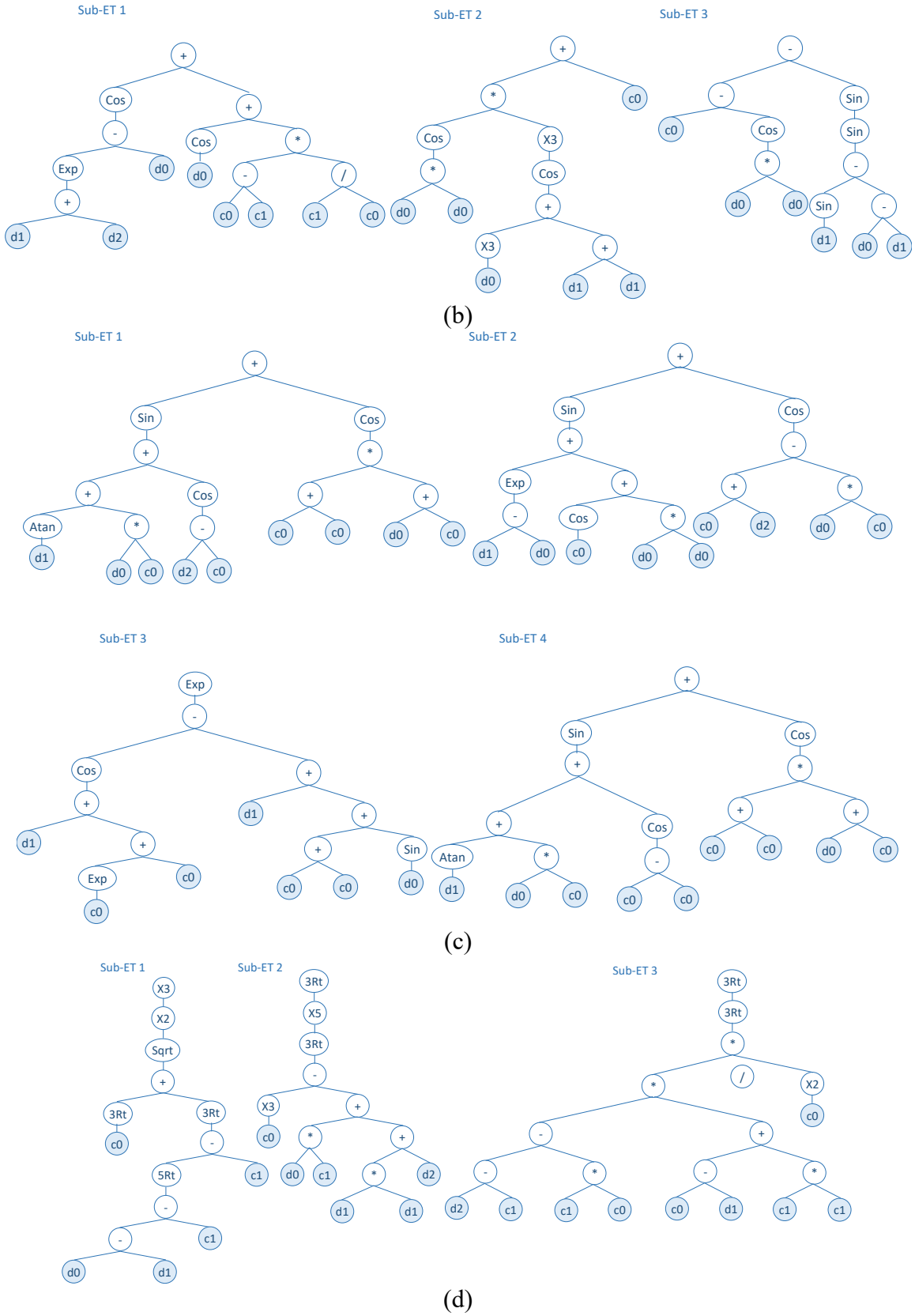

Fig. 4. Expression trees of (a) *GEP13*, (b) *GEP16*, (c) *GEP18* and (d) *GEP19* models for compressive strength.

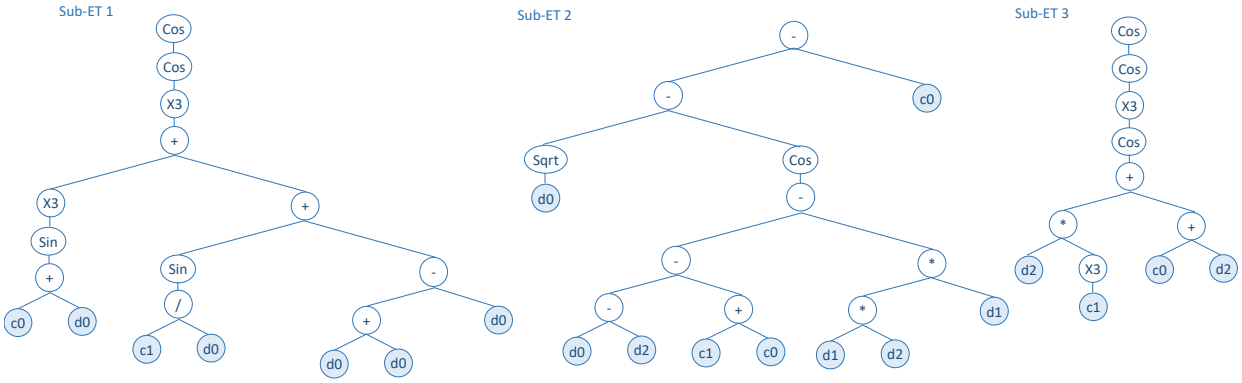
Sub-ET 1
Cos
Cos
X3
+
X3
+
Sin
Sin
-
+
/
+
c0
d0
c1
d0
d0
d0
Sub-ET 2
-
-
c0
Sqrt
Cos
d0
-
-
*
-
+
*
d1
d0
d2
c1
c0
d1
d2
Sub-ET 3
Cos
Cos
X3
Cos
+
*
+
d2
X3
c0
d2
c1

(a)

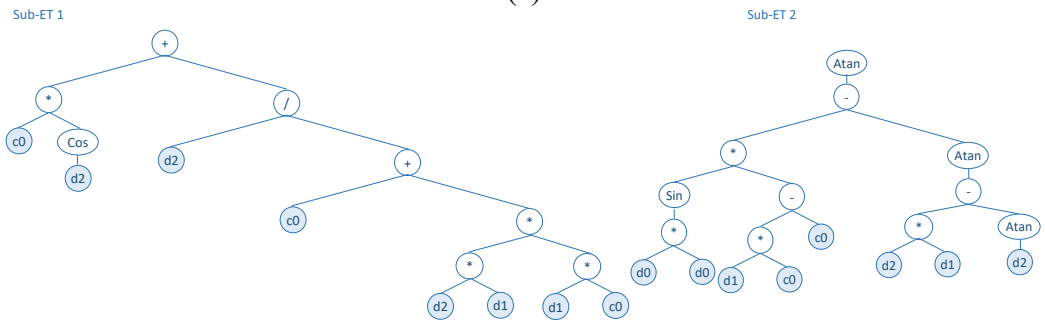
Sub-ET 1
+
*
/
c0
Cos
d2
+
d2
c0
*
*
*
d2
d1
d1
c0
Sub-ET 2
Atan
-
*
Atan
Sin
-
-
*
*
c0
Atan
d0
d0
d1
c0
d2
d1
d2

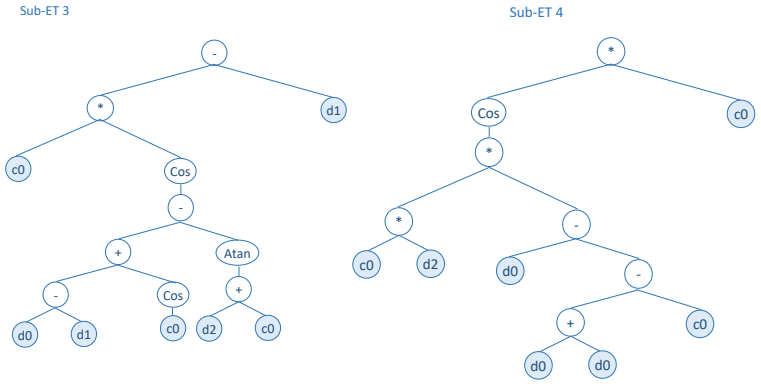
Sub-ET 3
-
*
d1
c0
Cos
-
+
Atan
-
Cos
+
d0
d1
c0
d2
c0
Sub-ET 4
*
Cos
c0
*
*
-
c0
d2
d0
-
+
c0
d0
d0

(b)

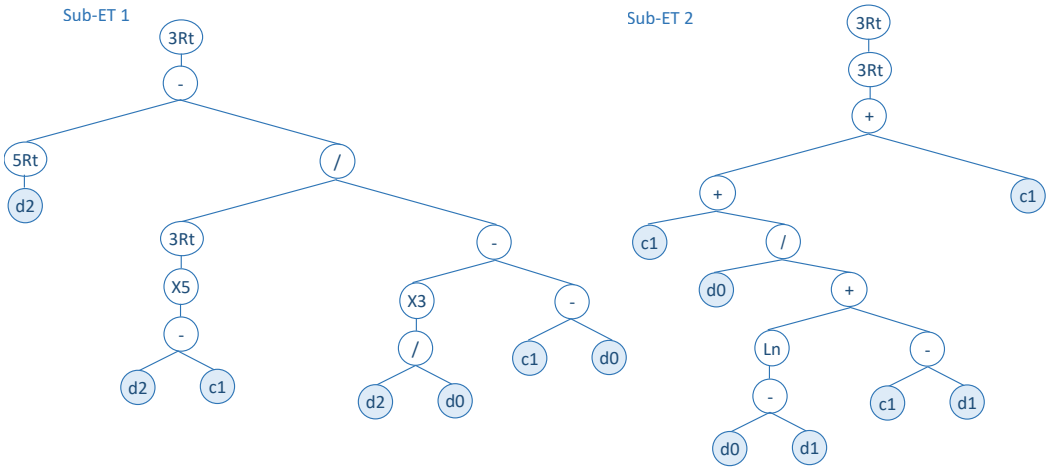
Sub-ET 1
3Rt
-
5Rt
/
d2
3Rt
-
X5
X3
-
-
d2
c1
/
c1
d0
d2
d0
Sub-ET 2
3Rt
3Rt
+
+
c1
c1
/
d0
+
Ln
-
-
c1
d1
d0
d1

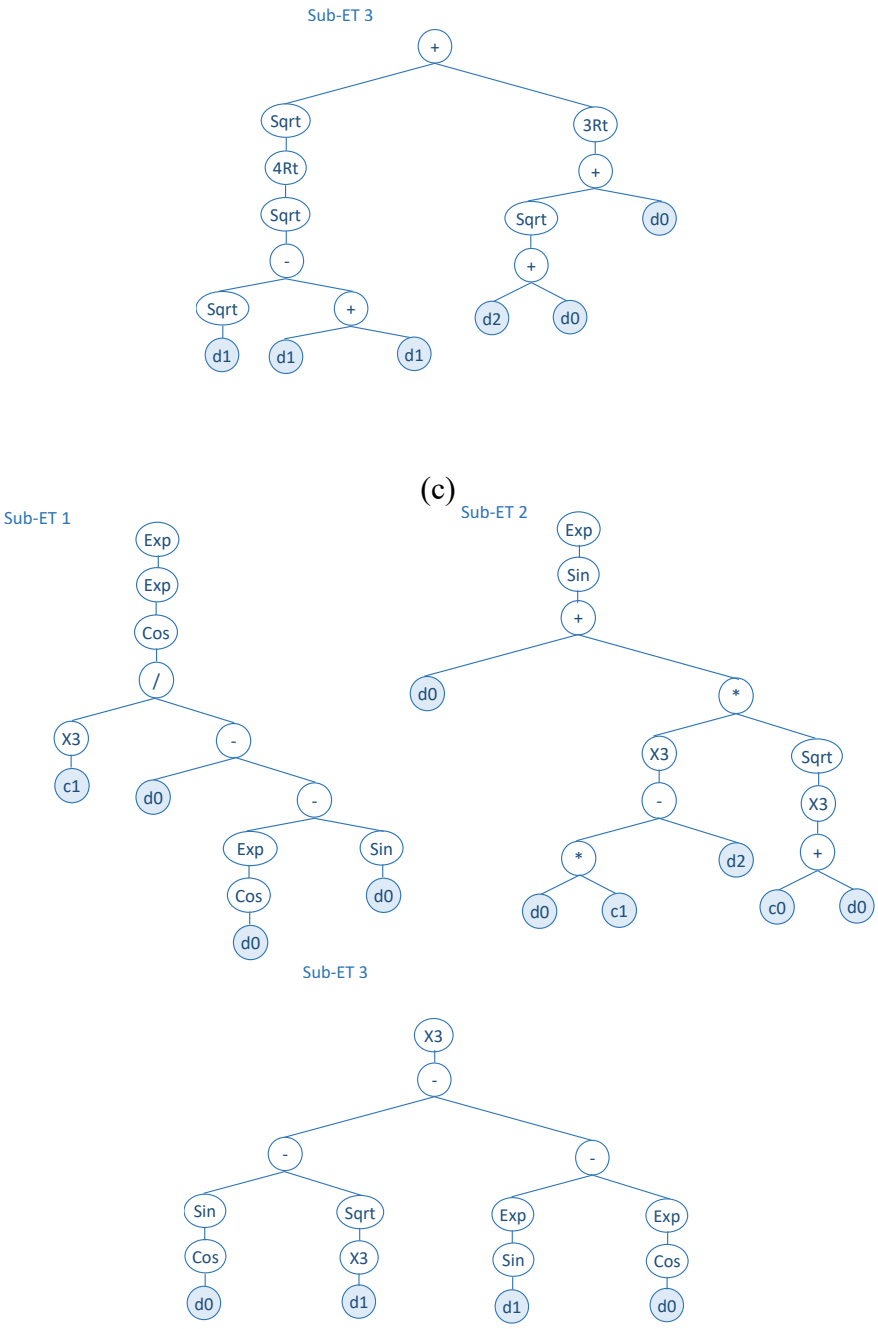

Fig. 5. Expression trees of (a) *GEP16*, (b) *GEP18*, (c) *GEP19* and (d) *GEP20* models for mass loss.

Figs. 6-9 show the linear least square fit, fit line, and R^2 values for the overall correlation of the best models. According to the figures, the proper correlation of the results of models *GEP16* and *GEP19* with the empirical results is clearly seen.

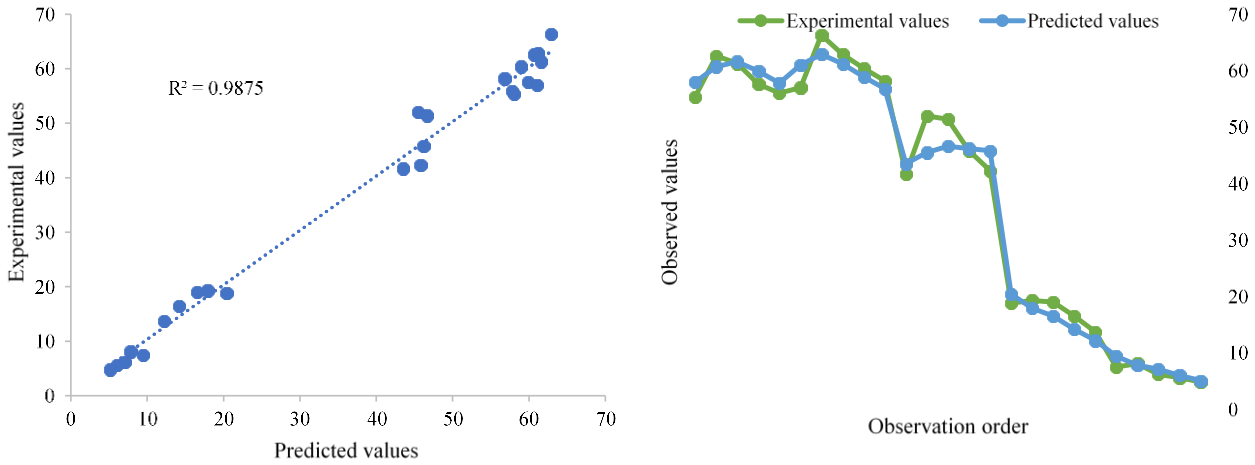

Fig. 6. Prediction versus empirical compressive strength scattering graph and curve fitting for *GEP16*.

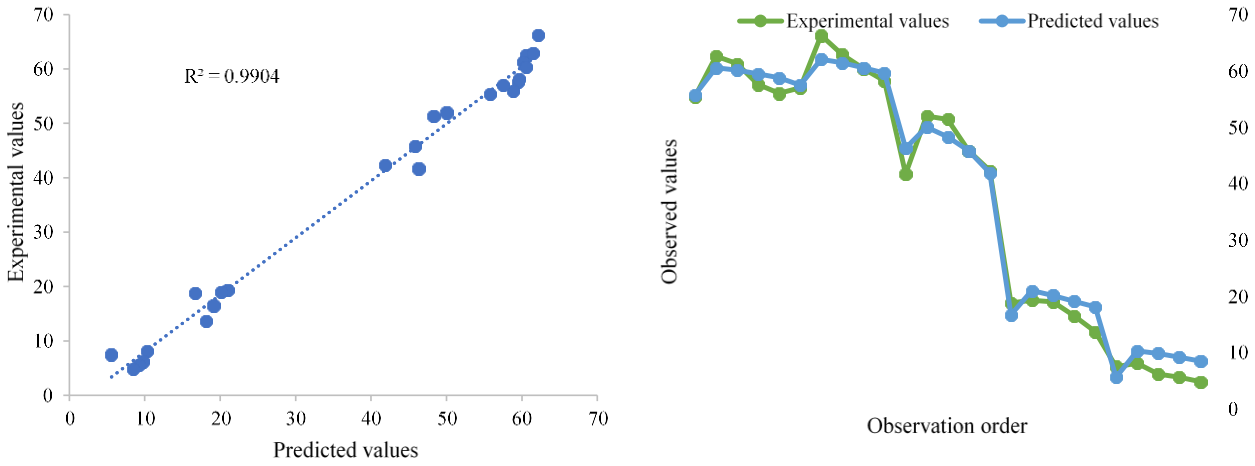

Fig. 7. Prediction versus empirical compressive strength scattering graph and curve fitting for *GEP19*.

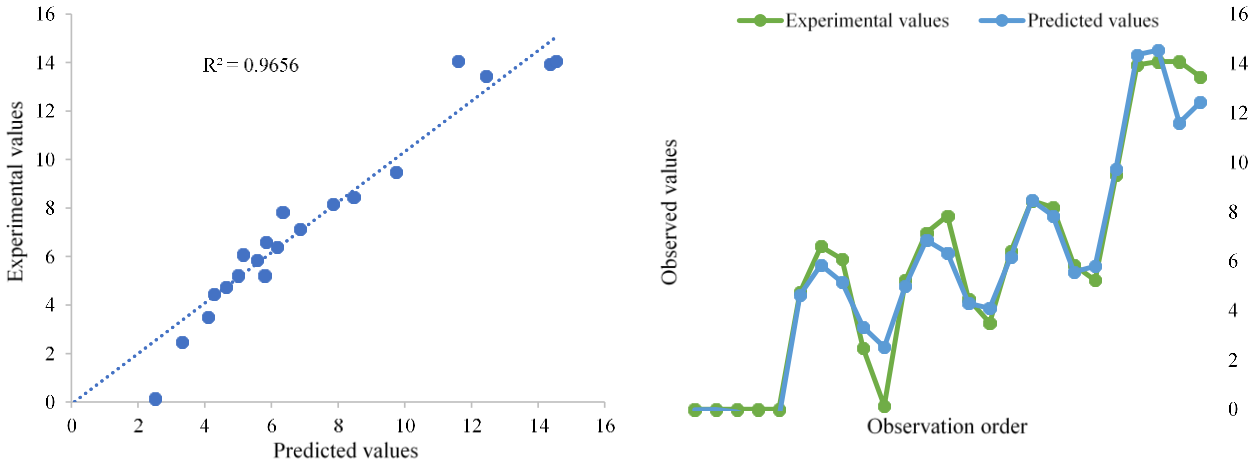

Fig. 8. Prediction versus empirical mass loss scattering graph and curve fitting for *GEP16*.

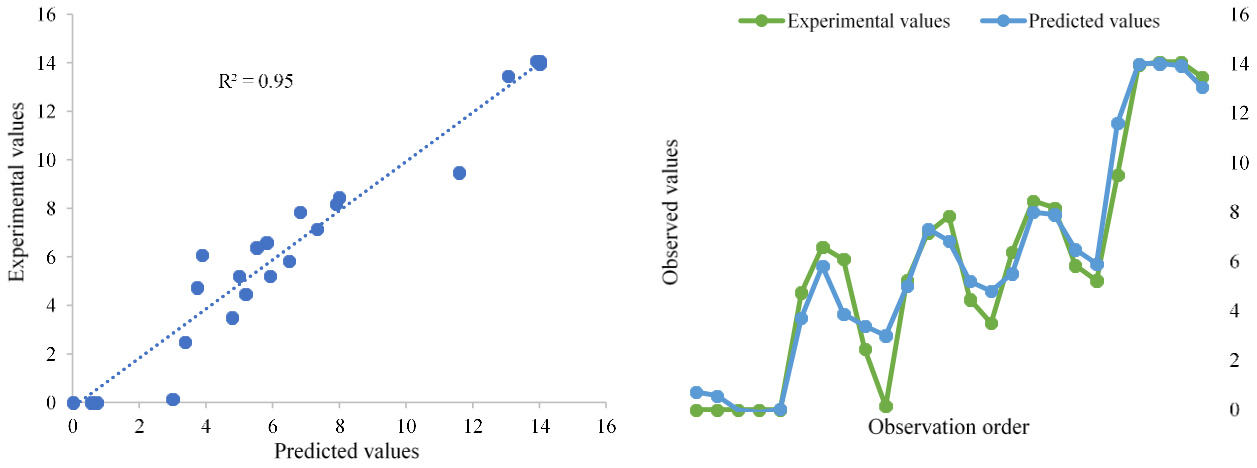

Fig. 9. Prediction versus empirical mass loss scattering graph and curve fitting for *GEP19*.

Tables 9 and 10 list the values of other error functions. These tables give the values of error functions for the training and testing sets. In terms of both strength and mass loss, *GEP16* and *GEP19* demonstrated the best performance. To evaluate agreement between the prediction and empirical results, R^2 is used, for which, values closer to 1 indicate good correlation between the model-predicted and empirical results [61]. Moreover, this function also determines how good a defined function fits on the data set. In this regard, the higher the value of R^2 in the training phase, the better the fitness of the final function. Nevertheless, this might result in the model deviation to the extent that it can no longer consider the hidden data. This way a significant difference between the errors of the training and testing occurs, which in turn leads to greater regression values in both training and testing sets.

Table 9
Statistical errors for compressive strength prediction.

Models	Phase	MAE	RMSE	RAE	RRSE	R^2	Models	Phase	MAE	RMSE	RAE	RRSE	R^2
GEP1	Training	3.254	5.430	0.150	0.240	0.956	*GEP11*	Training	8.633	13.141	0.398	0.568	0.765
	Validation	6.538	8.579	0.445	0.511	0.831		Validation	16.898	19.865	0.965	1.082	0.994
GEP2	Training	4.424	7.095	0.211	0.318	0.919	*GEP12*	Training	8.495	12.252	0.426	0.557	0.741
	Validation	3.342	4.572	0.164	0.204	0.964		Validation	6.608	9.888	0.307	0.438	0.819
GEP3	Training	2.639	4.465	0.147	0.219	0.962	*GEP13*	Training	3.007	3.904	0.143	0.173	0.972
	Validation	5.175	6.856	0.436	0.449	0.870		Validation	4.009	5.557	0.200	0.270	0.997
GEP4	Training	3.475	4.749	0.165	0.212	0.958	*GEP14*	Training	4.401	4.986	0.212	0.226	0.949
	Validation	8.658	10.065	0.558	0.511	0.809		Validation	3.145	4.031	0.190	0.194	0.991
GEP5	Training	3.890	8.436	0.194	0.385	0.919	*GEP15*	Training	3.389	4.190	0.163	0.190	0.964
	Validation	8.192	10.855	0.467	0.578	0.906		Validation	7.373	9.269	0.353	0.407	0.864
GEP6	Training	4.197	6.140	0.196	0.273	0.941	*GEP16*	Training	1.781	2.155	0.079	0.092	0.992
	Validation	7.619	8.950	0.608	0.554	0.841		Validation	3.050	3.573	0.250	0.244	0.941
GEP7	Training	4.053	5.113	0.195	0.230	0.951	*GEP17*	Training	8.159	8.980	0.407	0.411	0.835
	Validation	4.486	5.944	0.214	0.264	0.945		Validation	9.534	10.714	0.483	0.488	0.914
GEP8	Training	3.167	4.133	0.157	0.186	0.966	*GEP18*	Training	2.371	3.005	0.111	0.134	0.985
	Validation	4.433	6.460	0.239	0.324	0.947		Validation	3.606	4.834	0.219	0.238	0.955
GEP9	Training	3.189	5.455	0.152	0.247	0.953	*GEP19*	Training	1.903	2.296	0.110	0.116	0.989
	Validation	4.904	5.972	0.356	0.333	0.975		Validation	2.991	3.198	0.186	0.157	0.987
GEP10	Training	4.148	5.801	0.205	0.267	0.936	*GEP20*	Training	3.367	4.258	0.161	0.187	0.965
	Validation	4.391	5.044	0.187	0.208	0.964		Validation	6.252	7.317	0.352	0.385	0.996

Table 10
Statistical errors for mass loss prediction.

Models	Phase	MAE	RMSE	RAE	RRSE	R^2	Models	Phase	MAE	RMSE	RAE	RRSE	R^2
GEP1	Training	1.354	2.156	0.350	0.448	0.859	*GEP11*	Training	1.429	2.682	0.418	0.618	0.718
	Validation	1.696	2.102	0.651	0.650	0.844		Validation	3.007	3.677	0.681	0.701	0.849
GEP2	Training	1.568	2.350	0.418	0.504	0.808	*GEP12*	Training	1.429	2.682	0.418	0.618	0.501
	Validation	1.421	2.324	0.455	0.691	0.630		Validation	3.007	3.677	0.681	0.701	0.849
GEP3	Training	1.285	2.067	0.334	0.431	0.856	*GEP13*	Training	1.282	1.442	0.347	0.315	0.901
	Validation	2.694	3.369	1.063	1.073	0.989		Validation	3.145	3.392	0.954	0.777	0.546
GEP4	Training	2.013	3.321	0.559	0.728	0.641	*GEP14*	Training	1.323	1.546	0.365	0.339	0.820
	Validation	2.487	3.242	0.838	0.757	0.801		Validation	2.064	2.605	0.613	0.595	0.729
GEP5	Training	1.249	1.949	0.334	0.410	0.871	*GEP15*	Training	1.621	1.789	0.437	0.387	0.850
	Validation	3.166	3.553	2.089	1.956	0.902		Validation	0.665	0.957	0.201	0.232	0.985
GEP6	Training	1.485	2.256	0.453	0.529	0.817	*GEP16*	Training	0.478	0.701	0.138	0.158	0.975
	Validation	2.451	3.081	0.522	0.576	0.927		Validation	1.032	1.359	0.254	0.280	0.979
GEP7	Training	1.421	2.368	0.398	0.526	0.793	*GEP17*	Training	0.904	1.098	0.223	0.225	0.913
	Validation	2.566	3.295	0.696	0.703	0.789		Validation	1.781	2.105	0.878	0.829	0.453
GEP8	Training	1.516	2.507	0.452	0.582	0.702	*GEP18*	Training	0.784	0.965	0.236	0.226	0.952
	Validation	1.548	2.291	0.352	0.438	0.996		Validation	1.820	2.432	0.403	0.460	0.886
GEP9	Training	0.965	1.687	0.288	0.401	0.872	*GEP19*	Training	0.730	0.940	0.234	0.229	0.948
	Validation	3.873	4.177	0.790	0.781	0.501		Validation	0.757	1.309	0.142	0.228	0.964
GEP10	Training	1.083	1.728	0.270	0.350	0.887	*GEP20*	Training	1.002	1.474	0.254	0.304	0.910
	Validation	2.718	2.977	1.549	1.427	0.119		Validation	2.814	2.923	1.658	1.376	0.863

In general, more sophisticated models give greater values since they have more tries and generations; hence, a goal was to achieve less complexity. In most developed models, R^2 had a greater value in training set compared with the testing set. In this regard, R^2 for the strength predictions changed in the range of 0.741-0.992 for the training set and in the range of 0.809-0.997 for the testing set. Further, for mass loss prediction, the values of this function changed in the ranges of 0.501-0.975 and 0.261-0.996 for the training and testing sets, respectively.

Altogether, the statistical differences between empirical and prediction results were small. Hence, to predict the strength and mass loss of slag-based GPM incorporating RCA under heat, all the developed models are applicable. Additionally, a reduction occurs in the efficiency of the models with an increase in the MAE, RMSE, RAE, and RRSE values. It is seen that the values of RMSE, RAE, MAE, and RRSE are greater for the training compared with the testing in several models. For compressive strength, *GEP11*, *GEP12*, and *GEP17* and for mass loss, *GEP4*, *GEP10*, and *GEP12* had high errors, suggesting their performance reduction. However, for compressive strength, *GEP13*, *GEP16*, *GEP18*, and *GEP19* and for mass loss, *GEP16*, *GEP18*, *GEP19*, and *GEP20* had the smallest errors in both training and testing sets. Hence, the higher prediction ability of the latter eight models compared with the former six models is concluded.

For the strength models, the lowest and highest values of the RMSE error function were 2.155 and 19.865 in the training of *GEP16* and testing of *GEP11*, respectively. Also, for the mass loss models, the lowest and highest values of the above function were 0.556 and 4.177 in the training of *GEP18* and testing of *GEP9*, respectively. Nevertheless, the difference between the lowest and highest values was relatively notable for MAE. In this regard, for compressive strength, the lowest value of MAE was 1.781 in the training of *GEP16*, whereas, the highest value was 16.898

in the testing of *GEP11*. Also, for the mass loss, the corresponding lowest and highest values were 0.478 in the training of *GEP16* and 3.873 in the testing of *GEP9*, respectively.

Altogether, the results establish the applicability of GEP to predict mass loss compressive strength. The applicability of this approach for compressive strength has already been established by previous researchers [65,66].

5. Conclusions

It is well known that the compressive strength is the most important property of all concretes. In this study, for the first time, the GEP approach was used to evaluate the impact of the elevated temperatures on the eco-friendly geopolymer mortar (GPM) containing recycled concrete aggregate and propose formulas for its properties. Here, 20 models with different levels of input variables were proposed for estimating the compressive strength of GPM containing RCA. For running the models, data of experimental results were obtained from the experimental program. Most models yielded proper results in agreement with the empirical results. Another reason for GEP applicability for predicting compressive strength is the values of statistical error functions (R^2, MAE, RMSE, RAE, RRSE). In this regard, statistical differences between empirical and predicted results were small. Thus, the proper performance of all the models in predicting the compressive strength and mass loss of eco-friendly slag-based GPM incorporating RCA exposed to elevated temperatures is resulted. Moreover, based on the values of statistical errors, *GEP16* and *GEP19* had the best performance in terms of predicting both compressive strength and mass loss. The results of these two models correlated properly with the empirical results. This paper establishes that GEP can be used properly to predict the compressive strength and mass loss of eco-friendly GPM containing RCA and offer effective explicit formulas for many civil engineering problems. This approach can be used in future works to predict other properties of GPM containing RCA.

References

[1] J. Xie, Y. Guo, L. Liu, Z. Xie, Compressive and flexural behaviours of a new steel-fibre-reinforced recycled aggregate concrete with crumb rubber, Constr. Build. Mater. 79 (2015) 263–272. https://doi.org/10.1016/j.conbuildmat.2015.01.036.

[2] A. Shishegaran, F. Daneshpajoh, H. Taghavizade, S. Mirvalad, Developing conductive concrete containing wire rope and steel powder wastes for route deicing, Constr. Build. Mater. 232 (2020) 117184. https://doi.org/10.1016/j.conbuildmat.2019.117184.

[3] S. Kou, C. Poon, Effect of the quality of parent concrete on the properties of high performance recycled aggregate concrete, Constr. Build. Mater. 77 (2015) 501–508. https://doi.org/10.1016/j.conbuildmat.2014.12.035.

[4] N.A. Madlool, R. Saidur, M.S. Hossain, N.A. Rahim, A critical review on energy use and savings in the cement industries, Renew. Sustain. Energy Rev. 15 (2011) 2042–2060. https://doi.org/10.1016/j.rser.2011.01.005.

[5] E. Worrell, L. Price, N. Martin, C. Hendriks, L.O. Meida, Carbon dioxide emissions from the global cement industry, Annu. Rev. Energy Environ. 26 (2001) 303–329. https://doi.org/10.1146/annurev.energy.26.1.303.

[6] R.J. Thomas, S. Peethamparan, Alkali-activated concrete: Engineering properties and stress–strain behavior, Constr. Build. Mater. 93 (2015) 49–56. https://doi.org/10.1016/j.conbuildmat.2015.04.039.

[7] T. Luukkonen, Z. Abdollahnejad, J. Yliniemi, P. Kinnunen, M. Illikainen, One-part alkali-activated materials: A review, Cem. Concr. Res. 103 (2018) 21–34. https://doi.org/10.1016/j.cemconres.2017.10.001.

[8] V. Bilek, J. Hurta, P. Done, L. Zidek, Development of alkali-activated concrete for structures – Mechanical properties and durability, Perspect. Sci. 7 (2016) 190–194. https://doi.org/10.1016/j.pisc.2015.11.031.

[9] E. Gartner, H. Hirao, A review of alternative approaches to the reduction of CO 2 emissions associated with the manufacture of the binder phase in concrete, Cem. Concr. Res. 78 (2015) 126–142. https://doi.org/10.1016/j.cemconres.2015.04.012.

[10] M.C.G. Juenger, F. Winnefeld, J.L. Provis, J.H. Ideker, Advances in alternative cementitious binders, Cem. Concr. Res. 41 (2011) 1232–1243. https://doi.org/10.1016/j.cemconres.2010.11.012.

[11] N.R. Rakhimova, R.Z. Rakhimov, A review on alkali-activated slag cements incorporated with supplementary materials, J. Sustain. Cem. Mater. 3 (2014) 61–74. https://doi.org/10.1080/21650373.2013.876944.

[12] A. Hossein Rafiean, E. Najafi Kani, A. Haddad, Mechanical and Durability Properties of Poorly Graded Sandy Soil Stabilized with Activated Slag, J. Mater. Civ. Eng. 32 (2020) 04019324. https://doi.org/10.1061/(ASCE)MT.1943-5533.0002990.

[13] M. Chi, Effects of dosage of alkali-activated solution and curing conditions on the properties and durability of alkali-activated slag concrete, Constr. Build. Mater. 35 (2012) 240–245. https://doi.org/10.1016/j.conbuildmat.2012.04.005.

[14] F. Collins, J.. Sanjayan, Microcracking and strength development of alkali activated slag concrete, Cem. Concr. Compos. 23 (2001) 345–352. https://doi.org/10.1016/S0958-9465(01)00003-8.

[15] T. Bakharev, J.G. Sanjayan, Y.-B. Cheng, Effect of elevated temperature curing on properties of alkali-activated slag concrete, Cem. Concr. Res. 29 (1999) 1619–1625. https://doi.org/10.1016/S0008-8846(99)00143-X.

[16] S.A. Bernal, R. Mejía de Gutiérrez, A.L. Pedraza, J.L. Provis, E.D. Rodriguez, S. Delvasto, Effect of binder content on the performance of alkali-activated slag concretes, Cem. Concr. Res. 41 (2011) 1–8. https://doi.org/10.1016/j.cemconres.2010.08.017.

[17] Y. Ding, J.-G. Dai, C.-J. Shi, Mechanical properties of alkali-activated concrete: A state-of-the-art review, Constr. Build. Mater. 127 (2016) 68–79. https://doi.org/10.1016/j.conbuildmat.2016.09.121.

[18] F.G. Collins, J.G. Sanjayan, Workability and mechanical properties of alkali activated slag concrete, Cem. Concr. Res. 29 (1999) 455–458. https://doi.org/10.1016/S0008-8846(98)00236-1.

[19] K.-H. Yang, A.-R. Cho, J.-K. Song, Effect of water–binder ratio on the mechanical properties of calcium hydroxide-based alkali-activated slag concrete, Constr. Build. Mater. 29 (2012) 504–511. https://doi.org/10.1016/j.conbuildmat.2011.10.062.

[20] B. Walkley, A. Kashani, M.-A. Sani, T.D. Ngo, P. Mendis, Examination of alkali-activated material nanostructure during thermal treatment, J. Mater. Sci. 53 (2018) 9486–9503. https://doi.org/10.1007/s10853-018-2270-z.

[21] R.J. Myers, S.A. Bernal, R. San Nicolas, J.L. Provis, Generalized Structural Description of Calcium–Sodium Aluminosilicate Hydrate Gels: The Cross-Linked Substituted Tobermorite Model, Langmuir. 29 (2013) 5294–5306. https://doi.org/10.1021/la4000473.

[22] E.T. Stepkowska, J.M. Blanes, F. Franco, C. Real, J.L. Pérez-Rodríguez, Phase transformation on heating of an aged cement paste, Thermochim. Acta. 420 (2004) 79–87. https://doi.org/10.1016/j.tca.2003.11.057.

[23] G.-F. Peng, Z.-S. Huang, Change in microstructure of hardened cement paste subjected to elevated temperatures, Constr. Build. Mater. 22 (2008) 593–599. https://doi.org/10.1016/j.conbuildmat.2006.11.002.

[24] M. Guerrieri, J. Sanjayan, Investigation of the Cause of Disintegration of Alkali-Activated Slag at Temperature Exposure of 50°C, J. Mater. Civ. Eng. 23 (2011) 1589–1595. https://doi.org/10.1061/(ASCE)MT.1943-5533.0000313.

[25] U.-M. Jumppanen, U. Diederichs, K. Hinrichsmeyer, Material properties of F-concrete at high temperatures, VTT Technical Research Centre of Finland, 1986.

[26] M.C. Chi, R. Huang, W.H. Lu, Strength and Resistance of Alkali-Activated Slag Concrete to High Temperature, Appl. Mech. Mater. 193–194 (2012) 431–434. https://doi.org/10.4028/www.scientific.net/AMM.193-194.431.

[27] L. Zuda, Z. Pavlík, P. Rovnaníková, P. Bayer, R. Černý, Properties of Alkali Activated Aluminosilicate Material after Thermal Load, Int. J. Thermophys. 27 (2006) 1250–1263. https://doi.org/10.1007/s10765-006-0077-7.

[28] L. Zuda, P. Rovnaník, P. Bayer, R. Černý, Thermal Properties of Alkali-activated Slag Subjected to High Temperatures, J. Build. Phys. 30 (2007) 337–350. https://doi.org/10.1177/1744259106075234.

[29] M. Guerrieri, J. Sanjayan, F. Collins, Residual compressive behavior of alkali-activated concrete exposed to elevated temperatures, Fire Mater. 33 (2009) 51–62. https://doi.org/10.1002/fam.983.

[30] M. Guerrieri, J. Sanjayan, F. Collins, Residual strength properties of sodium silicate alkali activated slag paste exposed to elevated temperatures, Mater. Struct. 43 (2010) 765–773. https://doi.org/10.1617/s11527-009-9546-3.

[31] X. Ren, L. Zhang, Experimental study of interfacial transition zones between geopolymer binder and recycled aggregate, Constr. Build. Mater. 167 (2018) 749–756. https://doi.org/10.1016/j.conbuildmat.2018.02.111.

[32] N.K. Bui, T. Satomi, H. Takahashi, Mechanical properties of concrete containing 100% treated coarse recycled concrete aggregate, Constr. Build. Mater. 163 (2018) 496–507. https://doi.org/10.1016/j.conbuildmat.2017.12.131.

[33] J.M.. Gómez-Soberón, Porosity of recycled concrete with substitution of recycled concrete aggregate, Cem. Concr. Res. 32 (2002) 1301–1311. https://doi.org/10.1016/S0008-8846(02)00795-0.

[34] P. Kathirvel, S.R.M. Kaliyaperumal, Influence of recycled concrete aggregates on the flexural properties of reinforced alkali activated slag concrete, Constr. Build. Mater. 102 (2016) 51–58. https://doi.org/10.1016/j.conbuildmat.2015.10.148.

[35] K. Parthiban, K. Saravana Raja Mohan, Influence of recycled concrete aggregates on the engineering and durability properties of alkali activated slag concrete, Constr. Build. Mater. 133 (2017) 65–72. https://doi.org/10.1016/j.conbuildmat.2016.12.050.

[36] S.C. Kou, C.S. Poon, M. Etxeberria, Residue strength, water absorption and pore size distributions of recycled aggregate concrete after exposure to elevated temperatures, Cem. Concr. Compos. 53 (2014) 73–82. https://doi.org/10.1016/j.cemconcomp.2014.06.001.

[37] S. Akkurt, G. Tayfur, S. Can, Fuzzy logic model for the prediction of cement compressive strength, Cem. Concr. Res. 34 (2004) 1429–1433. https://doi.org/10.1016/j.cemconres.2004.01.020.

[38] A. Shishegaran, H. Taghavizade, A. Bigdeli, A. Shishegaran, Predicting the Earthquake Magnitude along Zagros Fault Using Time Series and Ensemble Model, Soft Comput. Civ. Eng. 3 (2019) 67–77.

[39] G. Hosseini, Capacity Prediction of RC Beams Strengthened with FRP by Artificial Neural Networks Based on Genetic Algorithm, J. Soft Comput. Civ. Eng. 1 (2017) 93–98.

[40] H. Naderpour, A.H. Rafiean, P. Fakharian, Compressive strength prediction of environmentally friendly concrete using artificial neural networks, J. Build. Eng. 16 (2018) 213–219. https://doi.org/10.1016/j.jobe.2018.01.007.

[41] H. Naderpour, K. Nagai, P. Fakharian, M. Haji, Innovative models for prediction of compressive strength of FRP-confined circular reinforced concrete columns using soft computing methods, Compos. Struct. 215 (2019) 69–84. https://doi.org/10.1016/j.compstruct.2019.02.048.

[42] H. Naderpour, D. Rezazadeh Eidgahee, P. Fakharian, A.H. Rafiean, S.M. Kalantari, A new proposed approach for moment capacity estimation of ferrocement members using Group Method of Data Handling, Eng. Sci. Technol. an Int. J. 23 (2020) 382–391. https://doi.org/10.1016/j.jestch.2019.05.013.

[43] D. Rezazadeh Eidgahee, A.H. Rafiean, A. Haddad, A Novel Formulation for the Compressive Strength of IBP-Based Geopolymer Stabilized Clayey Soils Using ANN and GMDH-NN Approaches, Iran. J. Sci. Technol. Trans. Civ. Eng. 44 (2020) 219–229. https://doi.org/10.1007/s40996-019-00263-1.

[44] H. Naderpour, P. Fakharian, A synthesis of peak picking method and wavelet packet transform for structural modal identification, KSCE J. Civ. Eng. 20 (2016) 2859–2867. https://doi.org/10.1007/s12205-016-0523-4.

[45] M. Yazdani, F. Jolai, Lion Optimization Algorithm (LOA): A nature-inspired metaheuristic algorithm, J. Comput. Des. Eng. 3 (2016) 24–36. https://doi.org/10.1016/j.jcde.2015.06.003.

[46] M. Yazdani, M. Babagolzadeh, N. Kazemitash, M. Saberi, Reliability estimation using an integrated support vector regression – variable neighborhood search model, J. Ind. Inf. Integr. 15 (2019) 103–110. https://doi.org/10.1016/j.jii.2019.03.001.

[47] I.F. Kara, Empirical modeling of shear strength of steel fiber reinforced concrete beams by gene expression programming, Neural Comput. Appl. 23 (2013) 823–834. https://doi.org/10.1007/s00521-012-0999-x.

[48] I. Ebtehaj, H. Bonakdari, No-deposition sediment transport in sewers using gene expression programming, J. Soft Comput. Civ. Eng. 1 (2017) 29–53.

[49] A. Shishegaran, M. Saeedi, A. Kumar, H. Ghiasinejad, Prediction of air quality in Tehran by developing the nonlinear ensemble model, J. Clean. Prod. 259 (2020) 120825. https://doi.org/10.1016/j.jclepro.2020.120825.

[50] P. Fakharian, H. Naderpour, A. Haddad, A.H. Rafiean, D.R. Eidgahee, A proposed model for compressive strength prediction of FRP-confined rectangular column in terms of Genetic expression Programming (GEP), Concr. Res. (2018).

[51] M. Nematzadeh, A.A. Shahmansouri, M. Fakoor, Post-fire compressive strength of recycled PET aggregate concrete reinforced with steel fibers: Optimization and prediction via RSM and GEP, Constr. Build. Mater. 252 (2020) 119057. https://doi.org/10.1016/j.conbuildmat.2020.119057.

[52] F. C., Gene Expression Programming: Mathematical Modeling by an Artificial Intelligence. Springer, 2006.

[53] A. Abd Elhakam, A.E. Mohamed, E. Awad, Influence of self-healing, mixing method and adding silica fume on mechanical properties of recycled aggregates concrete, Constr. Build. Mater. 35 (2012) 421–427. https://doi.org/10.1016/j.conbuildmat.2012.04.013.

[54] A. Shishegaran, M.R. Khalili, B. Karami, T. Rabczuk, A. Shishegaran, Computational predictions for estimating the maximum deflection of reinforced concrete panels subjected to the blast load, Int. J. Impact Eng. 139 (2020) 103527. https://doi.org/10.1016/j.ijimpeng.2020.103527.

[55] ASTM, C33-18: Standard Specification for Concrete Aggregates, ASTM International, Philadelphia, PA, 2018, (n.d.).

[56] ASTM, C230-14: Standard specification for flow table for use in tests of hydraulic cement, ASTM International, West Conshohocken, PA, 2014., (n.d.).

[57] ASTM, C305-14: Standard Practice for Mechanical Mixing of Hydraulic Cement Pastes and Mortars of Plastic Consistency, ASTM International, West Conshohocken, PA, 2014., (n.d.).

[58] ASTM, C109-16a: Standard Test Method for Compressive Strength of Hydraulic Cement Mortars (Using 2-in. or [50-mm] Cube Specimens), ASTM International, West Conshohocken, PA, 2016., (n.d.).

[59] J.R. Koza, J.R. Koza, Genetic programming: on the programming of computers by means of natural selection, MIT press, 1992.

[60] C. Ferreira, Gene expression programming: a new adaptive algorithm for solving problems, ArXiv Prepr. Cs/0102027. (2001).

[61] A.A. Shahmansouri, H. Akbarzadeh Bengar, E. Jahani, Predicting compressive strength and electrical resistivity of eco-friendly concrete containing natural zeolite via GEP algorithm, Constr. Build. Mater. 229 (2019) 116883. https://doi.org/10.1016/j.conbuildmat.2019.116883.

[62] A.A. Shahmansouri, H. Akbarzadeh Bengar, S. Ghanbari, Compressive strength prediction of eco-efficient GGBS-based geopolymer concrete using GEP method, J. Build. Eng. 31 (2020) 101326. https://doi.org/10.1016/j.jobe.2020.101326.

[63] A.A. Shahmansouri, H. Akbarzadeh Bengar, S. Ghanbari, Experimental investigation and predictive modeling of compressive strength of pozzolanic geopolymer concrete using gene expression programming, J. Concr. Struct. Mater. 5 (2020) 92–117.

[64] GEPsoft GeneXproTools, Data Modeling & Analysis Software. https://www.gepsoft.com/, (n.d.).

[65] M. Sarıdemir, Genetic programming approach for prediction of compressive strength of concretes containing rice husk ash, Constr. Build. Mater. 24 (2010) 1911–1919. https://doi.org/10.1016/j.conbuildmat.2010.04.011.

[66] M. Sarıdemir, Empirical modeling of splitting tensile strength from cylinder compressive strength of concrete by genetic programming, Expert Syst. Appl. (2011). https://doi.org/10.1016/j.eswa.2011.04.239.